processes

MDPI

*Article*

# Adsorption and Desorption Behavior of Ectoine Using Dowex® HCR-S Ion-Exchange Resin

**Yu-Chi Wu [1], Yu-Hong Wei [2] and Ho-Shing Wu [1,*]**

[1] Department of Chemical Engineering and Materials Science, Yuan Ze University, 135 Yuan Tung Road Chung Li, Taoyuan 320315, Taiwan; s1095207@mail.yzu.edu.tw
[2] Graduate School of Biotechnology and Bioengineering, Yuan Ze University, 135 Yuan Tung Road Chung Li, Taoyuan 320315, Taiwan; yhwei@saturn.yzu.edu.tw
* Correspondence: cehswu@saturn.yzu.edu.tw; Tel.: +886-3-463-8800-2564

**Abstract:** Dowex® HCR-S ion-exchange resin was used to adsorb ectoine in a batch system under varying operation conditions in terms of contact time, temperature, pH value, initial concentration of ectoine, and type of salt. Six adsorption isotherm models (Langmuir, Freundlich, Temkin, Dubinin–Radushkevich, Sips, and Redlich–Peterson) and three kinetic models (pseudo-first-order, pseudo-second-order, and intraparticle diffusion) were used to investigate the ectoine adsorption mechanism of ion-exchange resin. According to the experimental results, the mechanism of ectoine adsorption using an ion exchanger includes the ion-exchange reaction and physisorption. Both the Langmuir and Freundlich models were found to have a high fitting. For the kinetic analysis, the pseudo-second-order and intraparticle diffusion models were suitable to describe the ectoine adsorption. Dowex® HCR-S resin has an average saturated adsorption capacity of 0.57 g/g and 93.6% of ectoine adsorption at 25~65 °C, with an initial concentration of 125 g/L. By changing the pH of the environment using NaOH solution, the adsorbed ectoine on the ion-exchange resin can be desorbed to 87.7%.

**Keywords:** ectoine; ion exchange; separation and purification; kinetic and isotherm simulation

**Citation:** Wu, Y.-C.; Wei, Y.-H.; Wu, H.-S. The Adsorption and Desorption Behavior of Ectoine Using Dowex® HCR-S Ion-Exchange Resin. *Processes* **2021**, *9*, 2068. https://doi.org/10.3390/pr9112068

Academic Editors: Nicola Gargiulo and Suresh K. Bhatia

Received: 16 September 2021
Accepted: 17 November 2021
Published: 18 November 2021



## 1. Introduction

In recent years, because of increasing ultraviolet ray exposure and changes in social awareness, people have gradually paid more attention to skin and health care products. Ectoine ($C_6H_{10}O_2N_2$) [(S)-2-methyl-1,4,5,6-tetrahydropyrimidine-4-carboxylic acid]) is a chemical with a potentially high value and promising biotechnology, agriculture, pharmaceutical, and cosmiceutical applications. With its strong water-binding ability, ectoine can have a long-term moisturizing effect on human skin that is better than that of glycerol and relieve inflammation symptoms in allergic conjunctivitis. Ectoine can also block and protect biomolecules from the exposure damage of UV radiation and oxidative stress. Cosmetics became the first commercial product containing ectoine, giving them super hydrophilic characteristics, anti-wrinkle effects, and delayed skin-aging effects. Ectoine, which is an extremolyte, maintains the osmotic balance to protect biomolecules and cell structures by forming and stabilizing protective water layers around them. It can also protect skin under conditions of extreme dehydration, heating, drying, and freezing [1,2]. Accordingly, ectoine works as a multifunctional agent and demonstrates protective effects for proteins, DNA, food, human cells, and tissues. Ectoine has potential in other fields as well, and further research and innovations are possible [3,4].

Ectoine is one of the most widely present compatible solutes throughout various halophilic and halotolerant microorganisms in a broad range of Gram-negative and Gram-positive bacteria, such as α- and γ-*Proteobacteria*, *Actinobacteria*, and *Firmicutes* [4,5]. Heterotrophic bacteria usually produce it in the genera *Halomonas*, *Halorhodospira*, *Vibrio*,

*Chromohalobacter*, and *Pseudomonas* of the γ-*Proteobacteria* class [4,6–8]. Commercially, ectoine is usually synthesized by a bioprocess technique called "bacterial milking" using the halophilic bacterium *H. elongata* [5,9]. At present, in order to meet the increasing demand for commercial-scale production of ectoine, batch culture, fed-batch culture, bacterial milking [3,10], or non-halophilic bacteria (e.g., *E. coli*) are used in the fabrication process. These methods avoid high-salinity concentration strategies that would cause corrosion damage to equipment and reduce growth rates. However, ectoine fabrication still suffers from low production, whether halophilic or non-halophilic bacteria are used, with ectoine titers of 65 g/L and a specific productivity of 1.16 g/L/h (120 mg/g/h) achieved [11]. Hence, the isolation and purification of ectoine is the most critical step in improving downstream processing and reducing manufacturing costs.

Owing to its broad applications, ectoine it is a highly priced chemical, with a current sales price of USD 100/g when provided by Echochemical, Taiwan. Whether ectoine production is performed by bacterial milking, leaky mutants, or recombinant genes on non-halophilic bacteria, the loss of ectoine from the downstream processes, such as during separation and purification, must be reduced. Because ectoine is a highly hydrophilic compound, current separation methods, such as solvent extraction and salt extraction, cannot easily separate it from the fermentation broth. It is challenging to separate ectoine with high purity and low loss using mass separation methods like extraction or energy separation methods like distillation. Kunte et al. reported the production stages of industrial production of the cell protectant ectoine to include fermentation, microfiltration, desalting, capture, and refining [3]. The capture stage includes cation exchange and crystallization. Hence, many researchers use ion-exchange technology to separate it [2,12]. Sauer et al. described the use of Dowex 50 WX8 cation-exchange resin ($Na^+$ form) packed in a 2.8 × 18 cm cation-exchange column to elute ectoine [10]. Fülberth et al. reported that the ion-exchange resins used in ectoine separation include Dowex Marathon C, Dowex HCR-S, Dowex50WX8, Amberlite IR 122, and Fractogel EMD SE Hicap (M) [13].

Ion exchange is an interface-based process that is particularly efficient for low-concentration systems, and it involves mass transfer without the creation of byproducts. There is currently little in the literature in terms of detailed research on ectoine kinetic and isotherm parameters using ion exchangers, nor their adsorption/desorption behavior. Therefore, this study aimed to find the optimal operating conditions for ectoine purification from an aqueous solution using an ion-exchange strategy and reveal the underlying adsorption/desorption mechanism. Adsorption experiments were designed in a batch system with alternations in reaction time, pH, type of salt, temperature, and initial ectoine concentration. The adsorption isotherm and kinetic study were used to understand the nature of the sorption process, depending on the adsorbent characteristics, and inform the design of industrial sorption columns. The desorption process was performed with changes in pH, temperature, and NaOH concentration, and the desorption mechanism, parameters, and cost evaluation are also discussed.

## 2. Materials and Methods

### *2.1. Materials*

Ectoine ((S)-2-methyl-1, 4, 5, 6-tetra-hydropyrimidine-4-carboxylic acid, CAS 96702-03-3, >95%) was purchased from Sigma-Aldrich, Munich, Germany; it was produced by the natural Gram-negative bacteria *Halomonas elongate*. Dowex® HCR-S is a strong acid, styrene-divinylbenzene cation-exchange resin (CAS 64082-73-1, mesh size: 20-50 mesh, ionic form: H, moisture: 50–56%, capacity: 4.8 meq/g, Sigma-Aldrich, Munich, Germany). Dowex®50WX8 is a strong acid, styrene-divinylbenzene cation-exchange resin (CAS 69011-22-9, mesh size: 100–200 mesh, ionic form: Na, moisture: 54%, capacity: 4.8 meq/g, Sigma-Aldrich, Munich, Germany). HCl (35%) and NaOH (97%) were purchased from SHOWA (Tokyo, Japan). NaCl (99.8%) was purchased from Sigma-Aldrich (Munich, Germany). The water was deionized. All reagents were used as received, except for the resin.

Pretreatment of Resin

The resin (10 g) was washed using deionized water (20 mL) at least three times until the residual solution became colorless. The resin was regenerated using 15% HCl (120 mL) with a flow rate of 120 mL/h, then washed using deionized water (240 mL) with a flow rate of 240 mL/h. Next, we immersed the resin in acetone for 30 min to remove compounds such as alkylbenzenes, styrene, and uncrosslinked polymers, then dried the resin at 45 °C in an oven.

### *2.2. Batch Adsorption of Ectoine*

Batch adsorption experiments were conducted by mixing the ion-exchange resin (1 g) and ectoine solution (10 mL) in a 30 mL flask. The desired concentration of ectoine solution (1000 mg/L) was prepared by diluting from the stock solution in a 30 mL sample bottle. The concentration of the stock solution was 10,000 mg/L. The solution was agitated at 100 rpm at a selected temperature from 25 °C to 65 °C in a reciprocating water bath shaker (DK W-20, DENG YNG, Taipei,Taiwan). The mixture was shaken at a selected contact time, varying from 0.5 to 6 h for the kinetic experiment and 8 h for the equilibrium isotherm experiment. After adsorption, the samples were filtered through a polyvinylidene difluoride (PVDF) filter with a pore size of 0.45 μm. The residual concentration of ectoine in the filtrate was determined using HPLC with a wavelength of 210 nm.

Since ectoines are biomolecules and act as energy resources for microorganisms, they are easily decomposed when dissolved in water. Hence, capture or release of ectoine was performed in as short a time as possible.

The ectoine ion-exchange reaction is:

$$\overline{(R-SO_3^-)H^+} + \text{Ectoine ion}^+_{(aq)} \leftrightarrow \overline{(R-SO_3^-)\text{Ectoine ion}^+} + H^+_{(aq)} \quad (1)$$

The adsorption percentage of ectoine ions was calculated using Equation (2):

$$\text{Ectoine adsorption (\%)} = \left(\frac{C_0 - C_t}{C_0}\right) \times 100 \quad (2)$$

where $C_0$ is the initial ectoine concentration (mg/L) and $C_t$ is the ectoine concentration at time t (mg/L).

Equilibrium isotherm experiments were performed with various ectoine concentrations ranging from 1000 mg/L to 9000 mg/L at selected times. The amount of ectoine adsorbed per unit dried mass of adsorbent $q_e$ (mg/g) was calculated using Equation (3):

$$q_e = \frac{(C_o - C_e)V}{m} \quad (3)$$

where V is the volume of the solution (L); $C_0$ and $C_e$ are the initial and equilibrium concentrations of ectoine ion residuals in the aqueous solution (mg/L), respectively; and m is the dry weight of the adsorbent (g). SigmaPlot software (Systat Software, Inc., San Jose, CA, USA) was used to fit the nonlinear analysis of the isotherm models.

#### 2.2.1. Kinetic Study of Ectoine Adsorption

Resin (1 g) was added to a 10 mL ectoine solution (1000 mg/L) and agitated at 100 rpm at 35 °C in a reciprocating water bath shaker. The adsorbed rate of ectoine was investigated by measuring the ectoine ion concentration at predetermined time intervals using the HPLC method. The amount of adsorbed ectoine ions $q_t$ (mg/g) at time t (min) was calculated using Equation (4):

$$q_t = \frac{(C_0 - C_t)V}{m} \quad (4)$$

where $q_t$ is the adsorption capacity of ectoine in the resin phase at time t (mg/g); and $C_0$ and $C_t$ are the initial concentration and concentration of ectoine ion at time t (mg/L), respectively.

2.2.2. Preparation of Saturation Concentration of Ectoine in Ion-Exchange Resin

The saturation experiments were carried out in a 2 mL solution with 0.5 g dried resin (solution/resin = 4:1) under a selected concentration, referenced from the isotherm simulations. The saturation of ectoine in the resin was obtained, and subsequently, the desorption experiments proceeded for the next separation/purification procedure. The saturation capacity, $q_{sat}$ (g/g), of ectoine was calculated using Equation (5):

$$q_{sat} = \frac{(C_0 - C_e)V}{m \times 1000} \quad (5)$$

where $q_{sat}$ is the saturation capacity of ectoine in the resin phase at equilibrium (g/g).

2.2.3. Desorption of Ectoine

The desorption experiments were performed identically to the adsorption tests. Saturated resins were added to 10 mL of the desired desorbed agents, such as pure water, NaOH, or NaCl solution. The mixture of saturated resin and solution with a ratio of 0.1 g/mL was agitated at 100 rpm and at a selected temperature. The ectoine concentration of the solution was determined using HPLC. After the experiment, resins were collected for recycling in a new sorption-desorption cycle. The solution's pH value was adjusted with HCl (or NaOH). The pH was measured by using a digital pH meter (SUNTEX, New Taipei, Taiwan). Because ectoine possesses an isoelectric point with amino acids, the pH value was manipulated to transform the ectoine into the desired positively or negatively charged molecules. The desorption percentage of ectoine was:

$$\text{Ectoine desorption (\%)} = \left(\frac{C_e \cdot V}{q_{sat} \times 1000}\right) \times 100 \quad (6)$$

where $C_e$ is the concentration after reaching desorption equilibrium in the solution phase (mg/L).

*2.3. Swelling Index of the Ion Exchanger*

The dry resin was mixed with pure water at 25 °C for 2 h, and we then removed the surface water of the resin using filtration. The weight of the wet resin was measured. The swelling index, X, was calculated using Equation (7).

$$X = \frac{\text{Weight of wet resin} - \text{Weight of dry resin}}{\text{Weight of dry resin}} \quad (7)$$

*2.4. Determination of the Zeta Potential of Ectoine in the Solution*

Ectoine solution (10,000 mg/L) was diluted to the desired concentration using deionized water, and the pH value was adjusted using diluted HCl and NaOH solution. After this, we carefully washed it with deionized water and assembled the flow cell, where the solution contained analyte injects. Scanning of cells containing analytes at a high enough intensity or concentration was conducted to measure the zeta potential using NanoPlus (Norcross, GA, USA), with the software Particulate Systems (Norcross, GA, USA).

## 3. Models of Adsorption and Desorption

*3.1. Adsorption Kinetic Models*

Ion exchange and adsorption share various standard features regarding application of the batch and fixed-bed processes, which can be grouped as sorption for a unified treatment. These processes involve the transfer and equilibrium distribution of one or more solutes between a fluid phase and particles [14]. Adsorption kinetics are based on the relationship between the adsorbate–adsorbent and the reactor's operation in the adsorption

reaction, which plays a vital role in designing the plant column. Common adsorption kinetic equations are the pseudo-first-order model, pseudo-second-order model, and intraparticle diffusion model.

(i) Pseudo-first-order model

In 1898, Lagergren proposed a pseudo-first-order model describing a liquid–solid phase adsorption system, which showed that the adsorption rate is constructed based on the adsorption capacity [15]. The nonlinear form can be expressed as:

$$\frac{dq_t}{dt} = k_{pf}(q_e - q_t) \quad (8)$$

where $k_{pf}$ is the adsorption-rate constant ($min^{-1}$), $q_e$ is the equilibrium adsorption capacity (mg $g^{-1}$), and $q_t$ is the adsorption capacity (mg $g^{-1}$) at time t (min). We can plot the log rate ($q_e$–$q_t$) vs. t to calculate the adsorption rate constant [16].

(ii) Pseudo-second-order model

In 1995, Ho established a pseudo-second-order model in a batch reactor system [17]. The differential form is:

$$\frac{dq_t}{dt} = k_{ps}(q_e - q_t)^2 \quad (9)$$

where $k_{ps}$ is the adsorption-rate constant (g $mg^{-1}$ $min^{-1}$).

(iii) Intraparticle diffusion model

The intraparticle diffusion kinetic model focuses on the diffusion process and was proposed by Weber and Morris in 1962 [18]. During the solid–liquid adsorption reaction, the solute moves from the solution to the pores of the solid-phase adsorbent. This process is usually the rate-determining step in the entire adsorption reaction [16,19]:

$$q_t = k_{ip} t^{\frac{1}{2}} + C \quad (10)$$

where $k_{ip}$ is the intraparticle–diffusion constant (mg $g^{-1}$ $min^{-1/2}$) and C is the intercept constant (mg $g^{-1}$) of the model, which is proportional to the thickness of its boundary layer. The larger C is, the more significant the adsorption boundary layer's effect [19,20].

(iv) Elovich model

Elovich kinetics are widely applied to chemisorption (chemical reaction) to describe its mechanism and are suitable for heterogeneous adsorption systems. They were first formulated to describe the kinetics of the oxidation process and later developed for adsorption kinetics by Elovich and his collaborators from 1934 to 1939 [21]. Equation (11) covers an extensive range of adsorption systems with a mildly rising tendency.

$$\frac{dq_t}{dt} = \alpha e^{-\beta q_t} \quad (11)$$

where t is the adsorption time (min), α can be considered the initial adsorption rate (mg $g^{-1}$ $min^{-1}$) because ($dq_t/dt$) approaches α when $q_t$ approaches 0 [22], and β is the Elovich constant (g $mg^{-1}$).

In the kinetic system, the differential equation is integrated first. We can plot the integral form of the adsorption capacity, qt, with adsorption time. SigmaPlot software (Systat Software, Inc., San Jose, CA, USA) was used to fit the nonlinear analysis to obtain the parameters.

(v) Arrhenius activation energy

The adsorption activation energy is calculated from the Arrhenius equation:

$$\ln k = \ln A - \frac{E_a}{RT} \quad (12)$$

where k is the adsorption rate constant; A is the frequency factor and is independent of the temperature variable; $E_a$ is the adsorption activation energy (J $mol^{-1}$); R is the universal gas constant (8.314 J $mol^{-1}$ $K^{-1}$); and T is the solution temperature (K).

*3.2. Adsorption Isotherm Models*

(i) Langmuir isotherm

In 1916, Langmuir deduced the isothermal adsorption model based on the equilibrium between adsorption and desorption and concluded the relationship between the equilibrium adsorption, $q_e$, and the equilibrium concentration, $C_e$, of the liquid phase as a nonlinear form:

$$q_e = \frac{q_m K_L C_e}{1 + K_L C_e} \quad (13)$$

where $q_m$ is the maximum adsorption capacity of the monolayer (mg $g^{-1}$); $C_e$ is the equilibrium concentration in the solution (mg $L^{-1}$); and $K_L$ is the Langmuir equilibrium parameter (L $mg^{-1}$), defining the affinity of binding sites and the energy of sorption.

Furthermore, the constant $R_L$ can determine whether the adsorption process is spontaneous [23,24]. The $R_L$ equation is defined as:

$$R_L = \frac{1}{1 + K_L \times C_0} \quad (14)$$

(1) When $0 < R_L < 1$, adsorption proceeds in a favorable direction. (2) When $R_L > 1$, the adsorption process proceeds in an unfavorable direction. (3) When $R_L = 1$, the adsorption process is linear. (4) When $R_L = 0$, the adsorption process is irreversible [25–27]:

(ii) Freundlich isotherm

In 1906, Freundlich deduced an empirical formula based on isothermal equilibrium experiments which that widely employed to describe solid–liquid adsorption [28]. Freundlich isotherm theory supports reversible and nonideal adsorption on uneven surfaces. The Freundlich isotherm equation can be described as:

$$q_e = K_F \times C_e^{\frac{1}{n}} \quad (15)$$

where $K_F$ and n are Freundlich constants and the adsorption intensity, respectively.

(iii) Temkin isotherm

The Temkin isotherm is generally applied to describe monolayer adsorption behavior in a nonideal sorption system. By ignoring the extremely low and large value of concentrations, this isotherm assumes that the adsorption heat of all molecules in the layer would decrease, rather than logarithmically, with the increased coverage of the adsorbent surface. The Temkin isotherm model is:

$$q_e = \frac{RT}{b_T} \ln(A_T C_e) \quad (16)$$

where $b_T$ is the Temkin constant related to the sorption heat (J $mol^{-1}$) and $A_T$ is the Temkin isotherm constant related to equilibrium binding (L $mg^{-1}$).

(iv) Dubinin–Radushkevich isotherm

Dubinin and Radushkevich proposed the D–R isotherm adsorption model in 1947, which is a semi-empirical model. The D–R model assumes multilayer adsorption, which relates to Van der Waal's forces, and thus, it can be utilized in the simulation of the physisorption process [27]. The D–R isotherm equation is:

$$q_e = q_m[\exp(-B\varepsilon_d^2)] \quad (17)$$

where $q_m$ is the maximum adsorption capacity (mg $g^{-1}$); B is the energy constant ($mol^2$ $kJ^{-2}$); and $\varepsilon_d$ is the D-R constant ($mol^2$ $kJ^{-2}$). The D–R model is usually applied to distinguish adsorption types among chemisorption, physisorption, and ion exchange.

(v) Redlich–Peterson isotherm

Redlich–Peterson (R–P) is a hybrid isotherm with three parameters and is characterized by the combination of the Freundlich and Langmuir isotherm models. It can be described using Equation (18):

$$q_e = \frac{K_R C_e}{1 + \alpha_R C_e^g} \quad (18)$$

where $K_R$ is the R–P isotherm constant (L $g^{-1}$); $\alpha_R$ is the R-P isotherm constant (L $mg^{-1}$); and g is the R–P isotherm exponent.

(iv) Sips isotherm

Sips isotherm also features the heterogeneity factor $\beta_S$. The general expression of the Sips isotherm equation is:

$$q_e = \frac{K_S C_e^{\beta_s}}{1 + \alpha_S C_e^{\beta_s}} \quad (19)$$

where $K_S$ is the Sips isotherm constant (L $g^{-1}$); $\alpha_S$ is the Sips isotherm constant (L $mg^{-1}$); and $\beta_S$ is the Sips isotherm exponent. A summary of the adsorption isotherm and kinetic models is listed in Table 1.

**Table 1.** Summary of the adsorption isotherms and kinetic models.

| **Kinetic Model** | | **Ref.** |
|---|---|---|
| Elovich | $\frac{dq_t}{dt} = \alpha \exp(-\beta q_t)$ | [21] |
| Intraparticle diffusion | $q_t = k_{ip} t^{1/2} + C$ | [18] |
| Pseudo-first-order | $\frac{dq_t}{dt} = k_{pf}(q_e - q_t)$ | [15] |
| Pseudo-second-order | $\frac{dq_t}{dt} = k_{ps}(q_e - q_t)^2$ | [29] |
| **Isothermal model** | | **Ref.** |
| Dubinin–Radushkevich | $q_e = q_m e^{-B\varepsilon^2}$ | [30] |
| Freundlich | $q_e = K_F C_e^{1/n}$ | [28] |
| Langmuir | $q_e = \frac{q_m K_L C_e}{1 + K_L C_e}$ | [31] |
| Redlich–Peterson | $q_e = \frac{K_R C_e}{1 + \alpha_R C_e^g}$ | [32] |
| Sips | $q_e = \frac{K_S C_e^{\beta_s}}{1 + \alpha_S C_e^{\beta_s}}$ | [33] |
| Temkin | $q_e = \frac{RT}{b_T} \ln(A_T C_e)$ | [34] |

*3.3. Adsorption Thermodynamics*

In order to describe the thermodynamic behavior of ectoine ion sorption on cation-exchange resin, the thermodynamic parameters were calculated, including the Gibbs free energy (ΔG), entropy change (ΔS), and heat of adsorption (ΔH), using equilibrium constants at different temperatures (298–338 K). They can be obtained by using the following equations:

$$\Delta G = -\Delta H - T\Delta S \quad (20)$$

$$\Delta G = -RT \ln K_D \quad (21)$$

$$K_D = \frac{C_s}{C_e} \quad (22)$$

$$\ln K_D = \frac{-\Delta H}{RT} + \frac{\Delta S}{R} \quad (23)$$

where $K_D$ is the equilibrium distribution constant and $C_s$ (mg $L^{-1}$) and $C_e$ (mg $L^{-1}$) are the ectoine equilibrium concentration in the resin and aqueous phase, respectively. ΔH (kJ $mol^{-1}$), ΔG (kJ $mol^{-1}$), and ΔS (kJ $mol^{-1}$) can be calculated from a plot of ln $K_D$ versus 1/T. Inglezakis and Zorpas reported that ion exchange could be endothermic or exothermic with the involvement of heat of adsorption in the range of −24 to 38 kJ/mol, while the adsorption energy limits are found to be in the range of 0.6 kJ/ to 25 kJ/mol, and the activation energy is higher than 40 kJ/mol [35].

*3.4. Desorption Kinetic Models*

The external diffusion model (EDM) describes the desorption of ectoine from ion-exchange resin.

The EDM model assumes the ion-exchange reaction of ectoine molecules through the external film by a liquid-phase diffusion mechanism. The mass transfer is expressed as:

$$\frac{d}{dt} q_t = \frac{k_F}{\rho_P} (C_t - C_e) \quad (24)$$

where $q_t$ is the ectoine concentration on the resin (mg $g^{-1}$) at time t; $k_F$ is the volumetric mass-transfer coefficient in the external liquid film ($min^{-1}$); $\rho_P$ is the resin particle density (g/mL); and $C_t$ and $C_e$ are the ectoine concentrations, desorbed in the aqueous phase at time t [36].

## 4. Results and Discussion

*4.1. Adsorption of Ectoine Using Ion-Exchange Resin*

4.1.1. Effect of Types of Ion-Exchange Resin on the Adsorption of Ectoine

This study used two kinds of strong-acid cation-exchange resins (Dowex® 50WX8 and Dowex® HCR-S) to conduct adsorption experiments on ectoine in an aqueous solution. Figure 1 shows the effect of adsorption time on the strong-acid cation-exchange resin adsorption in a reciprocating water bath shaker. Dowex® 50WX8 showed a poor equilibrium adsorption efficiency in ectoine adsorption. The adsorption rate of ectoine using Dowex® 50WX8 was greater than that using Dowex® HCR-S. The swelling index (X) was calculated using Equation (7). The swelling index of Dowex® 50WX8 (X = 0.68) was lower than that of Dowex® HCR-S (X = 0.88). This finding explains why the adsorption capacity was low for Dowex® 50WX8, while the equilibrium time for Dowex® HCR-S was 120 min. Hence, Dowex® HCR-S was chosen as the candidate for adsorption, and the adsorption time was set at 8 h to reach the equilibrium state.

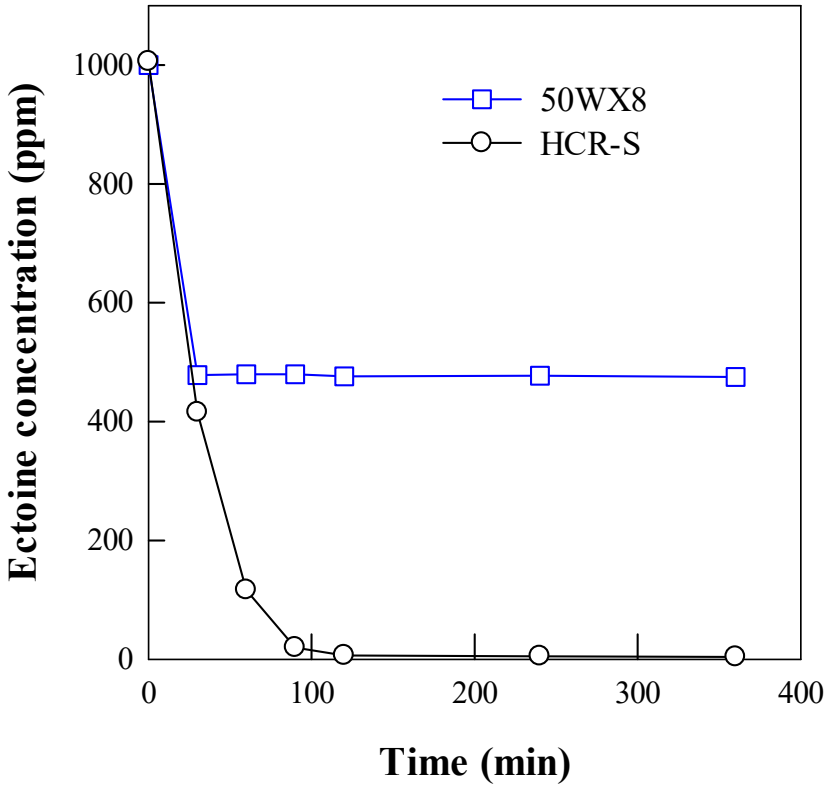


**Figure 1.** Effect of adsorption time on ectoine adsorption using ion-exchange resin (ectoine = 1000 mg/L, solution/resin = 10 mL/g, reaction time = 6 h, stirring rate = 100 rpm, temperature = 35 °C).

4.1.2. Effect of pH on Ectoine Adsorption

The solution's pH value is crucial to adsorption, especially for ion exchangers. Ectoine is a Zwitterion compound and can transform between cationic and anionic forms based on the pH, as shown in Figure 2. A zwitterion, also called an inner salt, contains an equal number of positively and negatively charged functional groups. Therefore, zwitterions are mostly electrically neutral; the whole molecule's net charge is zero. The isoelectric point is derived from its inner-salt structure. Hence, the pH can affect the adsorption capacity by changing the property of adsorbent and solution analytes. In this work, the initial pH of the solution was adjusted using HCl and NaOH, with and without the ion-exchange resin. Table 2 shows that the initial pH of the solution without ion-exchange resin does not affect the equilibrium adsorption capacity ($q_e$) of ectoine (mean = 9.83 mg/g). This demonstrates that the surface charge of both the exchanger and analyte is not affected by the surrounding pH, but the concentration gradient of $H^+$ inside the resin overwhelmed the solution's pH. The acidity of Dowex® HCR-S itself was pH 3.3 when 1 g of dry resin was immersed in 10 mL of neutral water. This demonstrates no effect on ectoine adsorption from adjusting the initial pH in the solution without resin. Therefore, we determined we should adjust the pH in the solution with resin before the experiment.

The pH of the solution with resin was adjusted using NaOH solution (3 M) with a long enough time for equilibrium to be reached. Table 2 indicates that the equilibrium adsorption capacity of ectoine ($q_e$) is affected by pH values. $q_e$ remained stable before the pH rose to over 3, slightly decreased at pH 4, and dramatically dropped at pH values over 4. After adsorption, the pH was reduced when it was lower than 4; in contrast, it increased when it was higher than 4. Therefore, the maximum adsorption was a 9.8 mg/g (0.07

meq/g) adsorption capacity of ectoine under pH < 3 when using an initial ectoine concentration of 1000 mg/L.

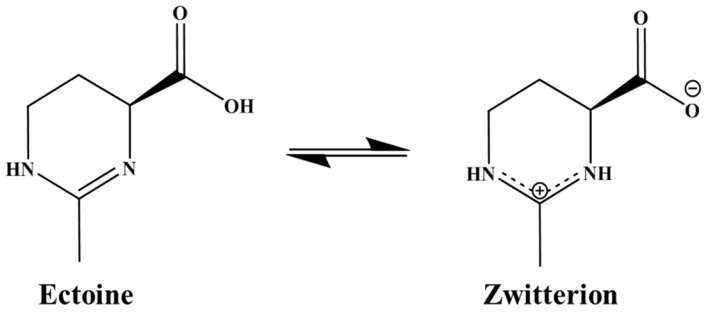


**Figure 2.** Zwitterion form of ectoine containing both acid and base centers and its isomer.

**Table 2.** Effect of pH in the solution with and without Dowex® HCR-S on ectoine adsorption.

| Initial pH without Resin | pH after Adsorption | $C_e$ (mg/L) | $q_e$ (mg/g) | Initial pH with Resin | pH after Adsorption | $C_e$ (mg/L) | $q_e$ (mg/g) |
|---|---|---|---|---|---|---|---|
| 2.00 | 1.98 | 15.73 | 9.84 | 2.00 | 1.95 | 19.90 | 9.80 |
| 3.00 | 2.82 | 15.94 | 9.84 | 3.00 | 2.90 | 18.04 | 9.82 |
| 4.00 | 3.18 | 14.44 | 9.86 | 4.00 | 3.80 | 80.23 | 9.20 |
| 5.00 | 3.29 | 16.87 | 9.83 | 5.00 | 6.70 | 740.76 | 2.59 |
| 6.00 | 3.30 | 20.79 | 9.79 | 6.00 | 6.89 | 869.34 | 1.31 |
| 7.00 | 3.33 | 15.23 | 9.85 | | | | |

Conditions: initial ectoine = 1000 mg/L, reaction time = 8 h, temperature = 35 °C, stirring rate = 100 rpm.

When the counterion $H^+$ of the resin is replaced with $Na^+$, $OH^-$ can neutralize the $H^+$ released from the resin to adjust the pH in the solution. Equilibrium pH can be attained in both the resin and aqueous phases. The results in Table 2 reveal that ectoine exists as a cationic form under pH < 4, known as its isoelectric point. The acidic nature of the resin results in preferential protonation of the ectoine molecules and thus more favorable ion exchange so that ectoine can exchange with hydrogen ions and maintain electroneutrality.

Aside from the surface-charged state of ectoine, the electrostatic affinity between the ion-exchanger ($R\text{-}SO_3^-$) and ectoine is assumed to be good. The pH in the solution will modify the adsorbent to become negatively charged to enhance the attraction to the desired ions, especially metal ions [37–39]. Dowex® HCR-S ion-exchange resin binding with the sulfonic group ($SO_3^-$) possesses a positive charge on the surface. This means that the surface charges of ectoine and the ion-exchanger have an opposite trend under pH < 4 in the aqueous medium.

#### 4.1.3. Zeta Potential in Ectoine Solution

The Zeta potential is defined as the magnitude of charge at the slipping plane, separating the mobile bulk fluid from the ionic layer attached to the particle surface. Since the surface charge is the primary key for using ion-exchange as the separation strategy of ectoine from bacterial broth, zeta potential analysis provides the results for the differentiation-charged situation on the particle surface under different pH conditions. Figure 3 shows that the pH of samples containing ectoine with a concentration of 2000 mg/L was titrated to pH = 2, 3, 4, 5, and 6 to determine the zeta potential. The isoelectric point of ectoine is located in the pH range between 3 and 4, close to 3.2.

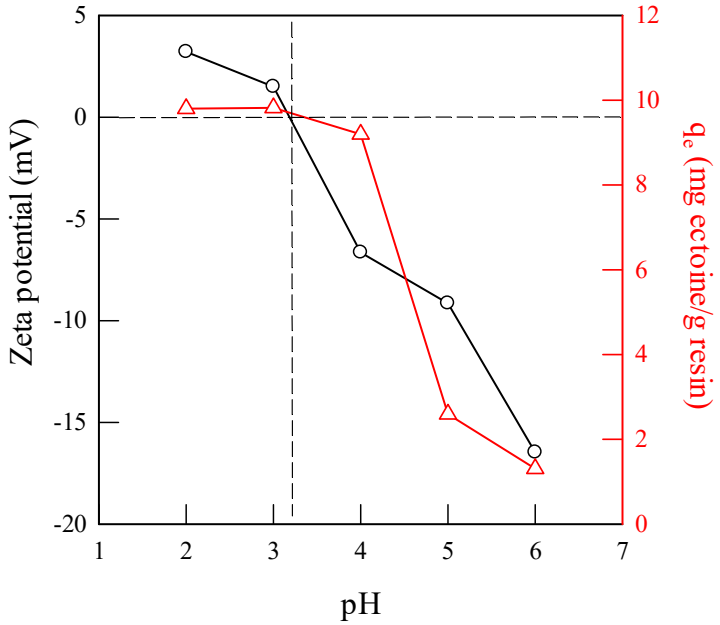


**Figure 3.** Plot of ectoine's zeta potential and adsorption capacity of ectoine on pH (Dowex® HCR-S resin/aqueous = 0.1 g/mL).

According to the structure of ectoine in Figure 2, ectoine carries a positive charge when the pH value is below its isoelectric point (pI) and carries a negative charge when the pH value is over its pI. The pI of ectoine is 3.2 when the zeta potential equals 0, as shown in Figure 3. Therefore, the adsorption conditions should be set at a pH value below 3.2 to apply the use of a cation-exchanger as the ectoine separation strategy.

The decline of adsorption capacity with increasing pH resulted from the change of ectoine's surface charge from positive to negative. A considerable electrostatic repulsion between ectoine ($Ect^-$) and the ion-exchanger surface ($R\text{-}SO_3^-$) under a high pH (>4) confirms the contribution of electrostatic interactions to the adsorption phenomenon. On the other hand, for pH values below 4, ectoine ions take on a cationic form, leading to an electrostatic attraction towards the ion-exchanger matrix, and an ion-exchange reaction occurs between hydrogen ions and ectoine ions. The result of the zeta potential of ectoine corresponds to that in Table 2. Moreover, we proved that the separation mechanism of ectoine using Dowex® HCR-S involves ion exchange and electrostatic force.

#### 4.1.4. Effect of Initial Ectoine Concentration

Figure 4a shows the isotherms of ectoine on Dowex® HCR-S at 25 °C and 65 °C with an initial ectoine concentration from 1000 mg/L to 9000 mg/L. The sequence of adsorption capacity for the effect of temperature was 65 °C > 25 °C > 55 °C > 35 °C > 45 °C. The ion-exchange process of ectoine onto Dowex® HCR-S was only slightly dependent on the operating temperatures because the differences in adsorption capacities among the different temperatures were small (<3%), as shown in Figure 4b. Consequently, the ion-exchange capacity of ectoine might depend on temperature, with a greater adsorptive uptake of ectoine at a higher temperature. The adsorption at 65 °C exhibited the best result in the range of 25 °C to 65 °C.

The adsorption that occurred can be divided into two temperature ranges: group I (25~45 °C) and group II (45~65 °C), as shown in Figure 4b. The adsorption performance decreased with rising temperatures in group I, while an enhancement of adsorption occurred with increasing temperatures in group II. For group I, the poor adsorption efficiency with increasing temperature can be explained by physisorption. The reduction in

equilibrium adsorption capacity ($q_e$) with increasing temperatures suggests a weak adsorption interaction between the ion-exchanger surface and the ectoine ion, supporting the physisorption assumption. Due to the higher mobility of ectoine ions, there was an increasing tendency for ectoine ions to escape from the ion-exchanger surface in the bulk solution. Hence, decreasing adsorption performance was observed as the temperature increased. Moreover, the thickness of the boundary layer decreases with higher temperatures, leading to poor adsorption efficiency [40].

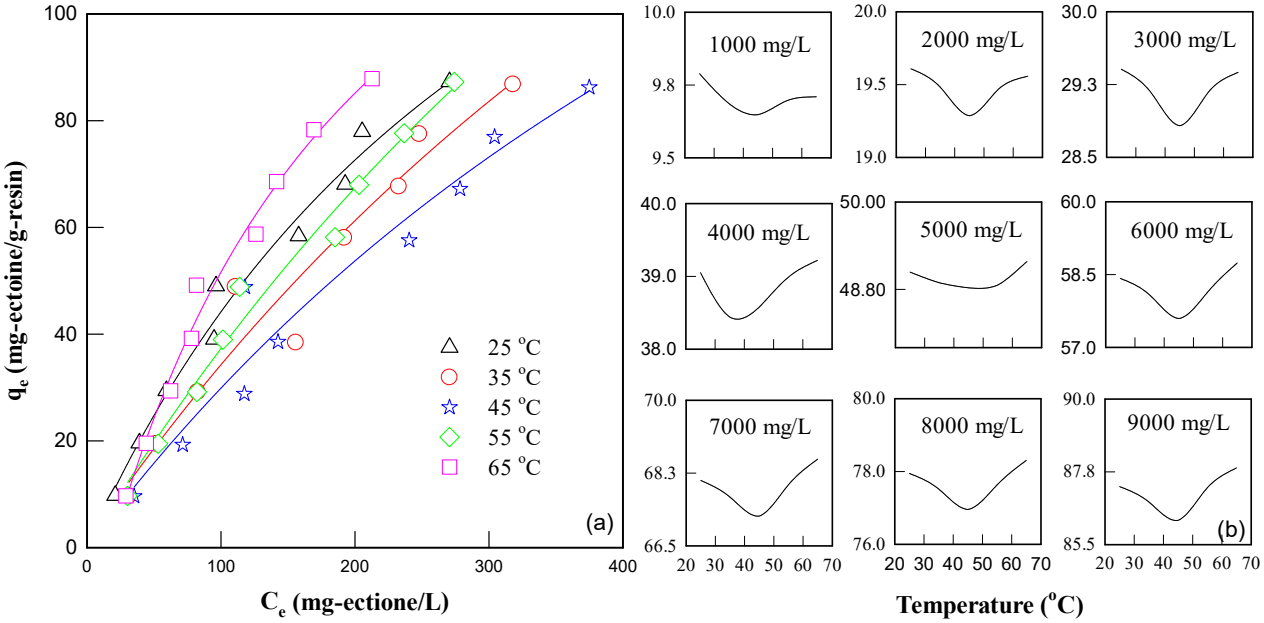


**Figure 4.** (**a**) Adsorption isotherm of ectoine using Dowex® HCR-S and (**b**) effect of adsorption capacity of ectoine on temperature at different initial ectoine concentrations (initial ectoine = 1000~9000 mg/L, dry resin/aqueous = 0.1 g/mL, agitated rate = 100 rpm, time = 8 h, temperature = 25~65 °C).

For group II, the adsorption capacity strengthened with increasing temperature. This phenomenon indicates that it is an endothermic reaction that is enhanced at higher temperatures. Additionally, it shows favorable intermolecular forces between ectoine ions and ion-exchange resin, making the adsorbate easier to adsorb. Chemisorption supports the adsorption in group II. Therefore, the adsorption of ectoine onto ion-exchange resin could be considered on the basis of two groups with the effect of temperature. Group I exhibited the characteristic of physisorption, but group II tended to show chemisorption.

#### 4.1.5. Isotherm Studies of Ectoine

This research used six models to describe the ion-exchange reaction: the Langmuir, Freundlich, Temkin, Dubinin–Radushkevich (D–R), Sips, and Redlich–Peterson (R–P) models. Nonlinear regression is a more general method that can be used to estimate model parameters [38]. For the three-parameter isotherm Sips and Redlich–Peterson models, nonlinear regression is easier than linearizing to find the optimal conditions. This study aimed to utilize a three-parameter isotherm because ectoine adsorption fits both the Langmuir and Freundlich models, while Sips and R–P isotherms, which are known Langmuir–Freundlich isotherms, combine Langmuir with Freundlich and thus exhibit both characteristics. Table 3 lists the parameters using all six isotherms for nonlinear regression. The R–P and Sips isotherms exhibited good fitting, like Langmuir and Freundlich, with the highest $R^2$ of 0.98 for R–P and 0.99 for the Sips model. Based on the parameters of the R–P isotherm, g was not equal to 1 but was close to it under some temperatures, which means

that ectoine adsorption does not follow the Langmuir isotherm fully. In other words, it is not a pure ion-exchange reaction.

The Langmuir equation was found to fit well to the experimental data, with a coefficient of determination ($R^2$) ranging from 0.94 to 0.99. The Langmuir constants ($R_L$) calculated by Equation (14) using the Langmuir equation, ranging from 0.038 to 0.454, were between 0 and 1, which indicates that the ion-exchange process proceeded in a favorable direction. The adsorption of ectoine increased concomitantly with the initial concentration.

**Table 3.** Isotherm parameters using nonlinear simulation for the adsorption of ectoine onto Dowex® HCR-S using the Freundlich, Langmuir, Dubinin–Radushkevich, Temkin, Redlich–Peterson, and Sips models.

| Temperature (°C) | Freundlich Model | | | Langmuir Model | | | | Dubinin–Radushkevich Model | | | Temkin Model | | |
|---|---|---|---|---|---|---|---|---|---|---|---|---|---|
| | n | $K_F$ (mg $L^{-1}$) | $R^2$ | $q_m$ (mg $g^{-1}$) | $K_L$ (L $mg^{-1}$) | $R^2$ | $R_L$ | $q_m$ (mg $g^{-1}$) | E [a] (kJ $mol^{-1}$) | $R^2$ | $b_T$ (J $mol^{-1}$) | $A_T$ (L $g^{-1}$) | $R^2$ |
| 25 | 1.35 | 1.43 | 0.98 | 201 | 0.0028 | 0.98 | | 79.7 | 0.011 | 0.87 | 81.0 | 0.051 | 0.95 |
| 35 | 1.22 | 0.80 | 0.95 | 299 | 0.0013 | 0.95 | | 78.3 | 0.009 | 0.82 | 79.1 | 0.035 | 0.91 |
| 45 | 1.24 | 0.74 | 0.95 | 259 | 0.0013 | 0.95 | 0.038–0.454 | 81.5 | 0.007 | 0.87 | 81.1 | 0.029 | 0.91 |
| 55 | 1.17 | 0.71 | 0.98 | 348 | 0.0012 | 0.98 | | 84.3 | 0.008 | 0.90 | 77.6 | 0.034 | 0.95 |
| 65 | 1.15 | 0.88 | 0.97 | 357 | 0.0016 | 0.97 | | 87.7 | 0.010 | 0.94 | 67.3 | 0.038 | 0.98 |

| Temperature (°C) | Redlich–Peterson Model | | | | Sips Model | | | |
|---|---|---|---|---|---|---|---|---|
| | $K_R$ (L $g^{-1}$) | $\alpha_R$ (L $mg^{-1}$) | g | $R^2$ | $K_S$ (L $g^{-1}$) | $\alpha_S$ (L $mg^{-1}$) | $\beta_S$ | $R^2$ |
| 25 | 0.58 | 0.0045 | 0.92 | 0.98 | 0.55 | 0.0028 | 1.00 | 0.98 |
| 35 | 0.52 | 0.0530 | 0.49 | 0.95 | 0.62 | 0.0009 | 0.88 | 0.98 |
| 45 | 0.37 | 0.0076 | 0.74 | 0.95 | 0.37 | 0.0013 | 0.98 | 0.95 |
| 55 | 0.41 | 0.0009 | 1.05 | 0.98 | 0.27 | 0.0012 | 1.11 | 0.98 |
| 65 | 0.51 | 9E-09 | 3.17 | 0.98 | 0.05 | 0.0004 | 1.63 | 0.99 |

dry resin = 1 g, initial ectoine = 1000~9000 mg/L, equilibrium time = 8 h, [a]: adsorption energy.

Figure 5 shows the direct prediction using the $q_e$ vs. $C_e$ diagram fitted with the Langmuir, Freundlich, Temkin, D–R, Sips, and R-P isotherms. One of the benefits of using nonlinear isotherm regression is direct simulation, showing the actual trend. A conclusion could be made that nonlinear regression is more general than linear fitting. Still, under some circumstances with restricted conditions, such as non-saturated curves, linearization provides easier and fast prediction with raw data.

Since nonlinear regression can reflect a more accurate and real system than linear regression, the nonlinear regression results exhibited a smaller and more precise range of data. In conclusion, the mechanism of ectoine capture using Dowex® HCR-S resin is not a pure ion-exchange reaction but a mixture of physisorption (van der Waals force) and ion exchange (Coulomb's force). This explains the result from Section 4.1.4 for the effect of temperature on ectoine adsorption, which could be divided into groups I (25~45 °C) and II (45~65 °C). Physisorption based on the van der Waals force was dominant when the temperature was below 45 °C, but chemisorption-like ion exchange based on the electrostatic force dominated when the temperature was above 45 °C.

Based on the isotherm results, the adsorption of ectoine is suggested to include physisorption and ion exchange. The strong hydrophilic force that emanates from the hydrogen bonds that exist between ectoine molecules explains physisorption. In terms of the ion exchange, ectoine as a cation had a higher affinity for exchanging sites than hydrogen ions. The following effect can influence the adsorption of ectoine by using ion-exchange resin: (i) hydrogen bonds existing between ectoine ions; (ii) the mass transfer of ectoine diffuses from the bulk solution to the boundary layer on the surface of the ion-exchange resin; (iii) the pore size of the ion-exchanger. As the temperature increased, physisorption based on hydrogen bonds became weaker due to the higher mobility and the increasing tendency for ectoine ions to escape from the surface of the ion exchanger. In contrast, chemisorption-like ion exchange became stronger when the temperature increased due to the higher mass transfer rate of intraparticle diffusion. Further, Dowex resin is a gel-type resin that is a microporous exchanger. Therefore, the rate-determining phase is either counterion interdiffusion within the ion exchanger (particle diffusion), or counterion interdiffusion in the adhering film (film diffusion).

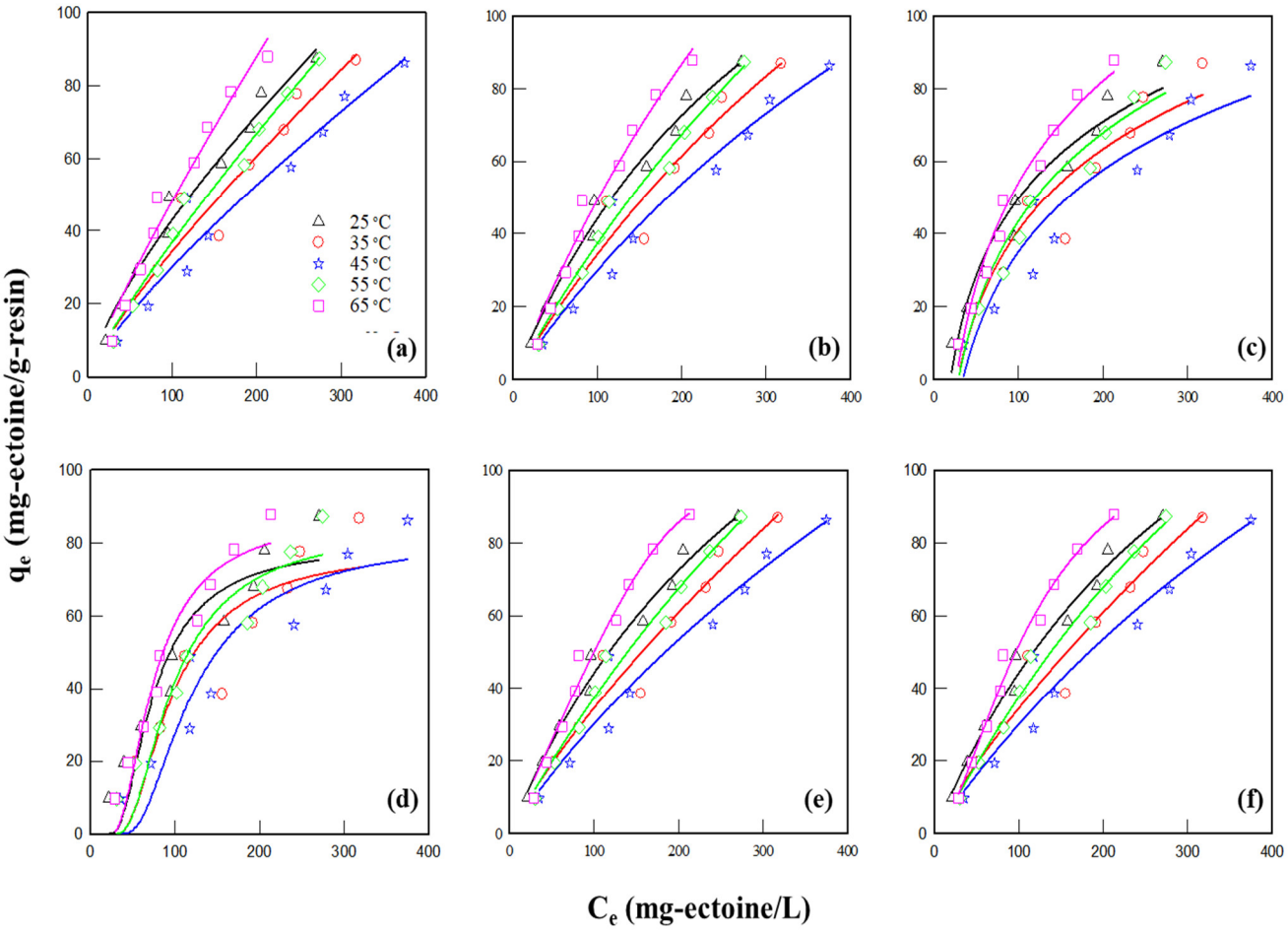


**Figure 5.** Nonlinear regression fitting curve using the isotherm models (**a**) Freundlich, (**b**) Langmuir, (**c**) Temkin, (**d**) D–R, (**e**) R–P, and (**f**) Sips for the simulation of ectoine adsorption.

#### 4.1.6. Effect of Adsorption Time

Adsorption kinetics involve the adsorption uptake concerning the time for measurements of the adsorbate diffusion in the pores of the adsorbent. This study conducted kinetic adsorption experiments in a batch system at different temperatures and adsorption times. The effect of contact time on ectoine adsorption was studied at pH 3.3 and agitating times of 30, 60, 90, 120, 240, and 360 min (Figure 6). The adsorption percentage of ectoine (%) was calculated by Equation (2) and was proportional to adsorption time until equilibrium was reached. Fast adsorption was spotted through the first 90 min of the process, reaching 91.7%, 97.5%, and 91.2% at 35 °C, 45 °C, and 55 °C, respectively. Fast adsorption might reflect the high accessibility of ectoine ions at the ion-exchange sites when the resin was immersed with ectoine molecules and swelled in the aqueous medium. Simultaneously, the stronger driving force resulting from the concentration gradient moved fast ectoine ions to the exchanging sites on the surface of the Dowex® HCR-S resin. On the other hand, with increasing time, the adsorption rate decreased and gradually reached equilibrium due to the crosslinking limit from the ion-exchange resin and the lower availability of the remaining exchange sites.

When the operating temperature was 45 °C, the adsorption rate was the highest; the adsorption percentage reached equilibrium faster than at 35 °C and 55 °C. However, there was no significant effect of temperature on the equilibrium adsorption percentage, which is close to 100% removal. Therefore, the effect of temperature is demonstrated in Figure 6: (1) the adsorption rate was influenced by different temperatures with the trend of 45 °C >

35 °C ≈ 55 °C; (2) there was no obvious effect of temperature on the equilibrium adsorption, which was almost 100% adsorption, resulting from the unsaturated adsorption of ectoine on the ion-exchange resin because of insufficient loading of the initial ectoine concentration.

Therefore, the adsorption of ectoine on the cation-exchange resin is affected by reaction time and temperature. A reaction time of 120 min is required to reach equilibrium. The adsorption rate was influenced by different temperatures, while the equilibrium adsorption did not significantly differ at different temperatures.

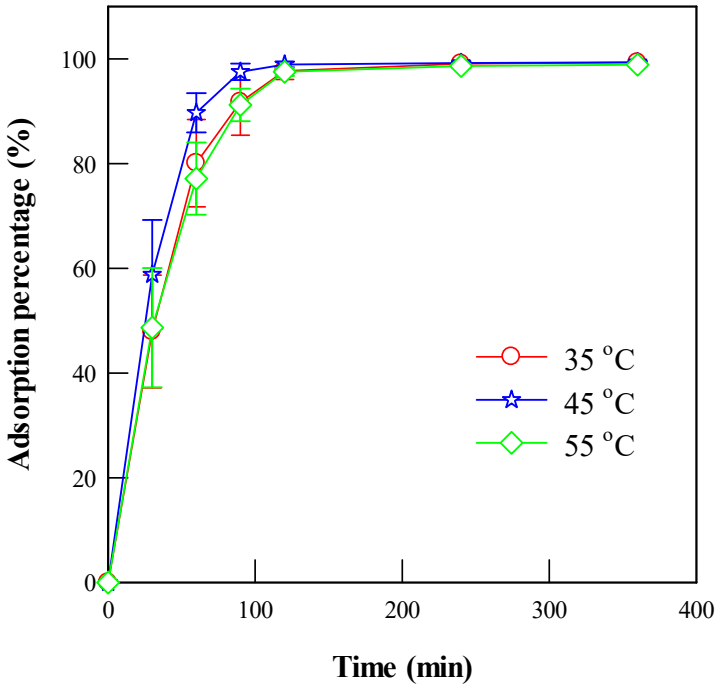


**Figure 6.** Effect of adsorption time on ectoine adsorption percentage at different temperatures (Dowex® HCR-S = 1 g, initial ectoine = 1000 mg/L, aqueous solution = 10 mL).

4.1.7. Adsorption Kinetics of Ectoine onto the Ion-Exchanger

Adsorption kinetics are a crucial factor in determining the mass-transfer constant and kinetics parameters. This information is essential for the design of an adsorbent-packed column in actual industrial applications. The adsorption kinetics simulation depicted the adsorbate's retention rate or release from the bulk solution to the solid-phase surface of adsorbents at a given adsorbent dose, temperature, flow rate, and pH [41]. When designing an adsorption system, the adsorption rate, adsorbent surface complexity, concentration of adsorbate, and flow rate can affect the adsorption kinetics.

The simulation results obtained by the pseudo-first-order model, pseudo-second-order model, Elovich equation, and intraparticle diffusion model are shown in Figure 7. The activation energy of the physisorption process was lower than 40 kJ/mol. The activation energy was between 24 and 40 kJ/mol for the ion-exchange reaction [35]. According to Table 4, the activation energies of the pseudo-second-order and intraparticle diffusion models were 36.5 kJ/mol and 35.1 kJ/mol, respectively. The pseudo-second-order model can describe the electrostatic interaction between ectoine and sulfonic groups ($SO_3^-$) covalently bonded in the ion-exchange matrix because it is related not only to ectoine ions or exchange sites but also to the attractions and repulsions between them.

Figure 7d shows two-step adsorption by plotting $q_t$ against $t^{1/2}$. The first half of the curve belongs to the diffusion during the solid-liquid adsorption process. The second half of the straight line is the saturation condition. The adsorption reaction mechanism usually consists of three consecutive steps, starting from the adsorption on the outer surface of the

solid phase, moving the solute in the liquid phase to the solid surface layer, and then performing intraparticle diffusion, transferring from the solid surface layer to the pores. The solute slowly moves from the large pores to the small pores to reach an equilibrium state among the pores. The intercept is usually a positive value, indicating a rapid adsorption reaction in a short period of time.

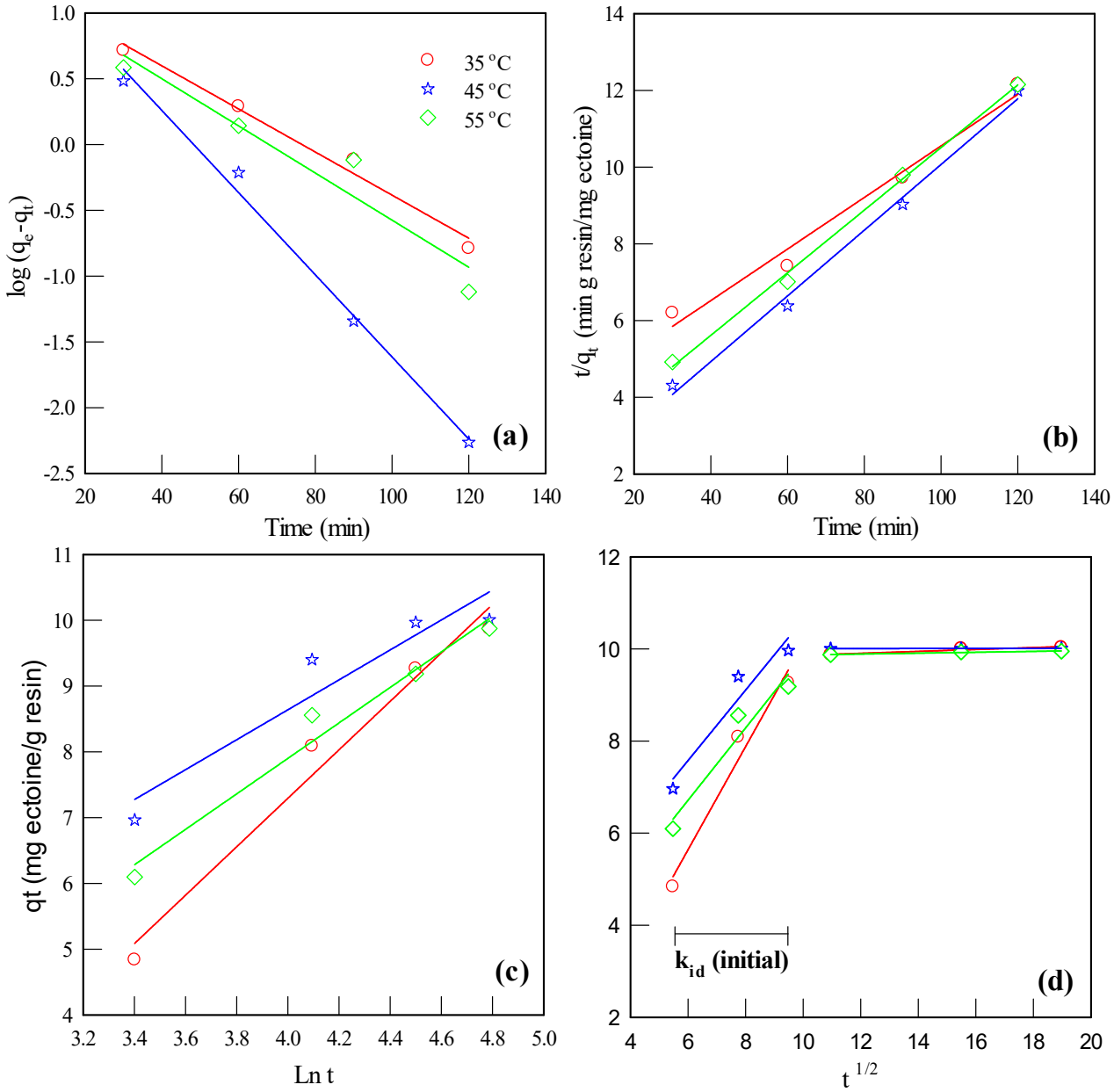


**Figure 7.** Regression analysis of the adsorption of ectoine by the (**a**) pseudo-first-order equation, (**b**) pseudo-second-order equation, (**c**) Elovich equation, and (**d**) intraparticle diffusion model.

**Table 4.** Kinetic parameters for ectoine ions using Dowex® HCR-S as the adsorbent.

| T (°C) | $q_e$ [a] (mg $g^{-1}$) | Pseudo-First-Order | | | | Pseudo-Second-Order | | | |
|---|---|---|---|---|---|---|---|---|---|
| | | $k_{pf}$ ($Min^{-1}$) | $q_e$ [b] (mg $g^{-1}$) | $R^2$ | $E_a$ (kJ $Mol^{-1}$) | $k_{ps}$ (g $mg^{-1}$ $Min^{-1}$) | $q_e$ [b] (mg $g^{-1}$) | $R^2$ | $E_a$ (kJ $Mol^{-1}$) |
| 35 | 10.03 | 0.04 | 18.00 | 0.98 | | 0.0012 | 14.90 | 0.97 | |
| 45 | 10.01 | 0.07 | 32.34 | 0.99 | 3.72 | 0.0049 | 11.67 | 0.99 | 36.5 |
| 55 | 9.95 | 0.04 | 16.50 | 0.92 | | 0.0028 | 12.25 | 1.00 | |

| T (°C) | Elovich | | | | Intraparticle diffusion | | |
|---|---|---|---|---|---|---|---|
| | α (mg $g^{-1}$ $min^{-1}$) | β (mg $g^{-1}$) | $R^2$ | $E_a$ (kJ $mol^{-1}$) | $k_{id}$(initial) (mg $g^{-1}$ $min^{1/2}$) | $R^2$ (initial) | E (kJ $mol^{-1}$) |
| | | | | | 1.12 | 0.97 | |
| 35 | 0.49 | 0.27 | 0.97 | | 0.77 | 0.93 | 35.1 |
| | | | | | 0.79 | 0.94 | |
| 45 | 1.86 | 0.44 | 0.90 | 23.1 | | | |
| 55 | 0.83 | 0.35 | 0.97 | | | | |

$k_{id}$ (initial): rate constant before equilibrium using the intraparticle diffusion model; a: experimental, b = simulated. Resin = 1g, ectoine = 1000 mg/L.

#### 4.1.8. Effect of Salt Concentration

Ectoine is produced using fermentation from halophilic and halotolerant bacteria; thus, salts, such as NaCl, occur in the ocean. While the liquid was maintained at a neutral pH, salt was dissolved in the ectoine solution at different concentrations to study ectoine adsorption with ion-exchange resin. Furthermore, the desorption was conducted after capturing ectoine with an ion-exchange resin. Figure 8 shows that the ectoine residual concentration increased with salt in the liquid phase. This shows that ectoine ions compete with sodium ions at the ion-exchange sites.

#### 4.1.9. Adsorption Thermodynamics

Equilibrium adsorption was used to investigate the thermodynamic properties of ectoine adsorption, and the thermodynamic parameters, including the equilibrium distribution coefficient ($K_D$), Gibbs free energy (△G), enthalpy (△H), and entropy (△S), were calculated. According to the results in Table 5, the negative ΔH values demonstrated that ectoine adsorption is an exothermic process at temperatures between 25 and 45 °C, whereas positive values revealed an endothermic reaction at temperatures between 45 and 65 °C. This supports the idea that ectoine adsorption in group I could be more favorable at lower temperatures and is a physisorption and exothermic process. In contrast, chemisorption in group II exhibits endothermic characteristics. Similarly, in group I, the values of ΔS were negative, indicating that the system's randomness at the boundary layer of a solid solution decreased during the adsorption process. In contrast, positive values of ΔS indicate that the randomness at the resin-solution interface increased. At all experiment temperatures, the values of ΔG were negative, showing that the adsorption process was spontaneous. The ΔG for physical adsorption is usually between −20 and 0 kJ $mol^{-1}$, while it is between −400 and −80 kJ $mol^{-1}$ for chemical adsorption. Ectoine adsorption had a ΔG of −14.6 kJ $mol^{-1}$ on average, indicating it was mostly physisorption. The heats of adsorption (△H) were -256 and 351 J/ mol, which corresponds to the heat range of adsorption of −24–38 kJ/mol [35].

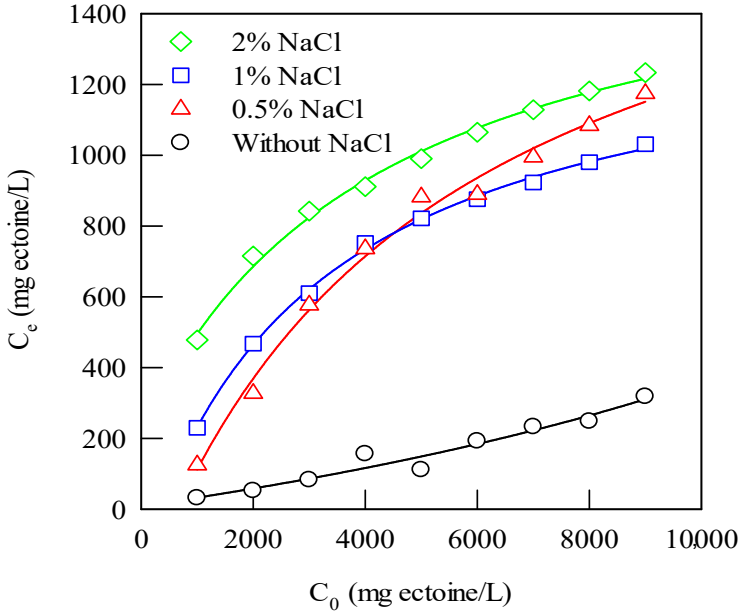


**Figure 8.** Effect of salt on adsorption of ectoine using a cation-exchange resin (Dowex® HCR-S = 1 g, initial ectoine = 1000–9000 mg/L, aqueous solution = 10 mL).

**Table 5.** Thermodynamic parameters of ectoine adsorption at different temperatures (group I = 25~45 °C; group II = 45~65 °C).

| $C_0$ (g/L) | ΔH (J/mol) | | ΔS (J/mol) | | ΔG (kJ/mol) | | | | |
|---|---|---|---|---|---|---|---|---|---|
| | I | II | I | II | 25 °C | 35 °C | 45 °C | 55 °C | 65 °C |
| 1 | −302 | 129 | −19.22 | 74.8 | −15.2 | −14.2 | −13.9 | −14.3 | −14.4 |
| 2 | −352 | 319 | −29.74 | 116.0 | −15.4 | −14.7 | −13.9 | −14.6 | −15.1 |
| 3 | −401 | 422 | −41.39 | 137.5 | −15.4 | −14.5 | −13.6 | −14.6 | −15.3 |
| 4 | −243 | 401 | −7.08 | 133.9 | −14.9 | −13.7 | −13.9 | −14.8 | −15.4 |
| 5 | −118 | 240 | 24.31 | 101.8 | −15.4 | −15.1 | −14.9 | −15.0 | −15.9 |
| 6 | −248 | 430 | −8.16 | 138.7 | −14.7 | −14.2 | −13.6 | −14.3 | −15.2 |
| 7 | −217 | 450 | −1.55 | 143.4 | −14.5 | −14.1 | −13.6 | −14.4 | −15.3 |
| 8 | −231 | 390 | −4.19 | 130.5 | −14.7 | −14.2 | −13.7 | −14.4 | −15.2 |
| 9 | −193 | 379 | 3.35 | 127.6 | −14.3 | −13.9 | −13.5 | −14.3 | −14.9 |
| Average | −256 | 351 | −9.30 | 122.7 | −14.6 | | | | |

*4.2. Saturation of Ectoine in the Ion-Exchange Resin*

Saturation experiments were carried out to confirm the maximum ectoine loaded in the cation-exchange resin and for further the desorption investigation. According to the isotherm results in Section 4.1.5, the predicted saturation capacities of ectoine on Dowex® HCR-S were 0.22–0.67 and 0.20–0.36 (g/g) based on the nonlinear Langmuir maximum adsorption capacity in Table 3, respectively. Therefore, the experiments were performed by mixing 0.5 g resin with 2 mL solution of ectoine, with the concentrations set as 0.12, 0.125, 0.135, 0.15, 0.17, and 0.20 g/mL. As shown in Figure 9a, there was no significant effect of initial concentration on ectoine saturation at 25 °C, and the adsorption capacity ranged from 0.55 to 0.60 (g/g). Therefore, the adsorption capacity can be confirmed as the saturation capacity ($q_{sat}$) since no more ectoine could be loaded with the amplification of the concentration gradient. Based on the results in Section 4.1.5, the mechanism of ectoine adsorption is not a pure ion exchange but a mixture of ion exchange, electrostatic force, and physisorption (van der Waals force). The Langmuir isotherm assumes adsorption occurs under a homogeneous system with monolayer adsorption, and thus, the predicted maximum adsorption lacks multilayer adsorption based on the Freundlich theory. Multilayer adsorption can be attributed to physisorption (van der Waals), with ectoine stacked

on the first layer sorption (ion exchange). The conclusion that the Sips isotherm, also known as the Langmuir–Freundlich model, can describe the ectoine adsorption by using Dowex® HCR-S shows that the experimental saturation capacity is larger than the Langmuir adsorption capacity. According to Figure 9b, the effect of temperature on ectoine saturation is not significant either, which means ectoine adsorption is not dependent on temperature.

According to Figure 9c, the resin weight did not affect the saturation capacity of ectoine in the ion-exchange resin significantly, and the ectoine-saturated capacity was around 0.56 (g/g) under the same temperature and initial ectoine concentration, which equaled an average of 3.9 (meq/g). The saturation percentage of the resin was 81.8% (=3.9/4.8) based on Dowex® HCR-S's total exchange capacity of 4.8 (meq/g).

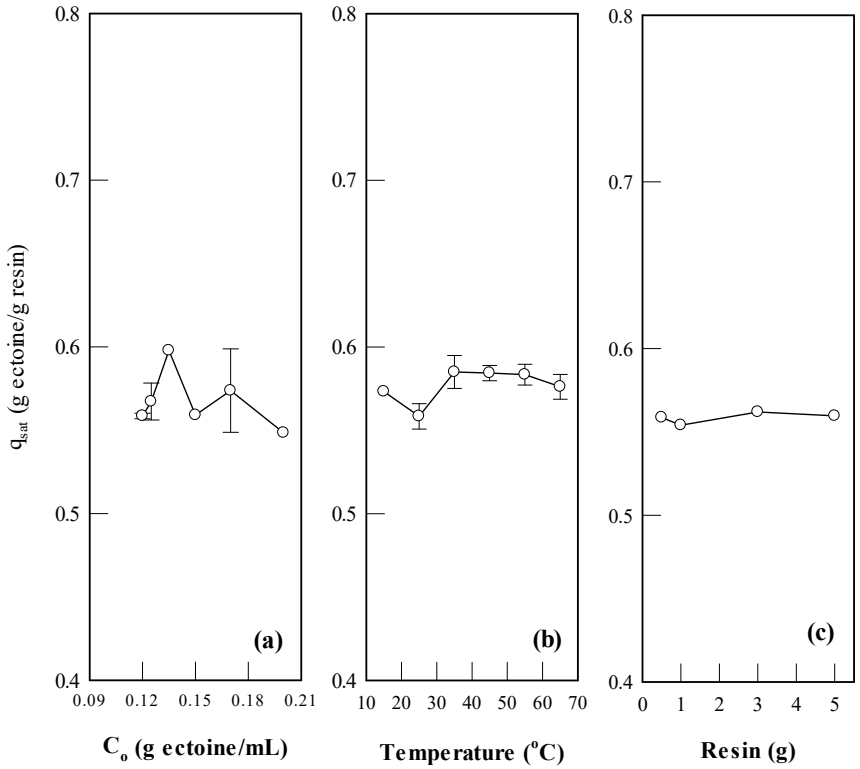


**Figure 9.** Effect of saturation adsorption capacity of ectoine using Dowex® HCR-S on (**a**) initial ectoine concentration, (**b**) temperature, and (**c**) resin dosage (aqueous/resin = 4 mL/g, agitation = 100 rpm, reaction time = 8 h).

### *4.3. Desorption of Ectoine from Saturated Ion-Exchange Resin*

Adsorption and ion exchange are feasible alternatives for the separation and purification processes. These interface-based methods involve mass transfer and are particularly efficient for low-concentration systems, such as ectoine produced from bacteria with low concentrations. In addition to a separate desired compound from the original stream, the recovery of adsorbate and adsorbent regeneration must be considered. The desorption of ectoine from the acidic cation-exchange resin was studied with different NaOH concentrations.

#### 4.3.1. Effect of pH on Ectoine Desorption

Based on the principle of using an ion exchanger to separate and purify amino acids, pH is the critical factor in modifying the analyte's surface charge to become cationic or anionic. To use a cationic-exchange resin in desorption, ectoine is supposed to transform to its anionic form to achieve electrostatic repulsion from the functional group ($SO_3^-$) fixed

in the ion-exchange matrix. Therefore, the pH should be set above the isoelectric point of ectoine to manipulate the charged property on the molecule surface. Based on Figure 3, the pI of ectoine was 3.2 and became the standard for designing the experiments. The experiments were performed under pH = 2, 3, 4, 5, and 6 to investigate the effect on ectoine desorption.

Table 6 shows that not much ectoine was released from the saturated resins with a desorption percentage <10%. This can be explained by the residual $H^+$ ions inside the saturated resin. Since the saturation capacity ranges from 0.55 to 0.60 g/g, the resin efficiency ranges between 80.6 and 87.9%, which means that 12.1 to 19.4% of hydrogen ions remain inside the resin. Therefore, the desorption capacity of 0.3~0.4 meq/g can be attributed to the salt desorption (exchanging with $Na^+$), and a more basic condition is required to allow the charged property of ectoine to change.

**Table 6.** Effect of pH on ectoine desorption from saturated Dowex® HCR-S resins.

| pH | $C_e$ (g/L) | $m_{ect,e}$ (g) | $m_{ect,e}$ (meq) | Desorption (%) |
|---|---|---|---|---|
| 2 | 5.42 | 0.06 | 0.42 | 9.96 |
| 3 | 4.05 | 0.04 | 0.31 | 7.44 |
| 4 | 3.72 | 0.04 | 0.29 | 6.84 |
| 5 | 3.58 | 0.04 | 0.28 | 6.58 |
| 6 | 3.99 | 0.04 | 0.31 | 7.33 |

$m_{ect,e}$ = mass of ectoine in solution at equilibrium. Condition: resin/aqueous = 0.1 g/mL; temperature: 20 °C; $q_{sat}$ = 0.60 g/g = 4.2 meq/g; time = 8 h.

#### 4.3.2. Effect of NaOH Concentration

The desorption equilibrium of ectoine released from saturated Dowex® HCR-S resin was found in a batch reactor, as shown in Figure 9. The sequence of temperatures for ectoine desorption was 15 °C ≈ 25 °C > 35 °C > 45 °C > 55 °C. The desorption performance was higher at lower temperatures. The desorption of ectoine was greatest at 15 °C, with 89.7% desorption. Theoretically, with a higher NaOH concentration, better desorption results could be obtained and a plateau reached due to the higher driving force provided with larger $OH^-$ concentrations. The best desorption performance was found at an NaOH concentration of ≈0.5 mol/L, as shown in Figure 10. Furthermore, the ectoine ions were transferred from the solid to the liquid phase when the eluent solution exchanged the ectoine molecules. This phenomenon is a consequence of mass transfer, which was boosted by the high concentration gradient between resin and solution phases and maximized by the ionic strength of the basic eluent. NaOH solution can promote a very high ectoine removal as a desorbed agent since even the lowest concentrations in the resin phase correspond to high concentrations in the solution, resulting in favorable desorption. When the NaOH concentration is larger than 0.5 mol/L, the desorption percentage of ectoine is decreased (Figure 10). This results from ectoine denaturation under extreme alkaline conditions.

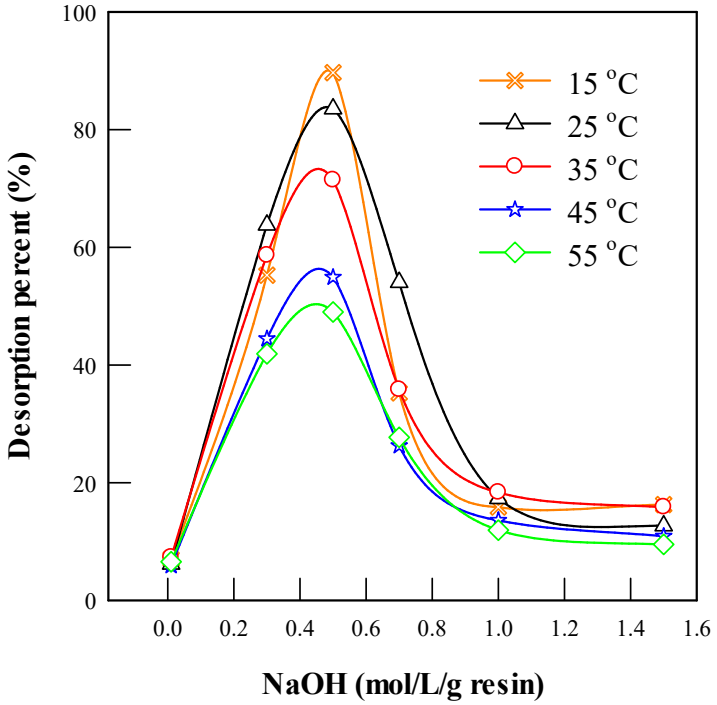


**Figure 10.** Effect of NaOH on the equilibrium desorption of ectoine using Dowex® HCR-S at different temperatures (saturated resin: 1 g, NaOH solution: 10 mL, time: 8 h).

#### 4.3.3. Effect of Desorption Time and Temperature

The effect of temperature on the equilibrium and the desorption kinetics using NaOH as an adsorbed agent was assessed to study the desorption rate. Figure 11 shows the effect of desorption time on the release of ectoine ions from Dowex® HCR-S resin. Ectoine ions were rapidly released from the acidic cation exchanger before 180 min, followed by slow desorption and equilibrium being attained. Desorption of ectoine ions was found to be proportional to the desorbed time before equilibrium was reached. The sequence of temperatures for ectoine desorption was 25 °C > 15 °C > 45 °C > 55 °C > 35 °C. This shows no trend for the temperature effect. Desorption and ion exchange may simultaneously control the reaction kinetics.

The desorption of ectoine released from ion exchangers in the first 180 min can be attributed to the strong driving force resulting from the concentration gradient of ectoine between the solid and solution phases and the fact that the resin was saturated first, which means the initial ectoine concentration was null ($C_0 = 0$) in the solution phase. At the same time, the desorbed agent NaOH played an essential role in converting ectoine from the cationic to anionic form in order to lose the electronic attraction and even repel the sulfonic functional group ($SO_3^-$) covalently fixed in the ion-exchanger matrix. On the other hand, the desorption process decreased as the reaction time increased. This can be explained by the structure of the ion-exchanger synthesized by polystyrene-divinylbenzene since cross-linking can hinder and slow down the immersion and swelling of resin.

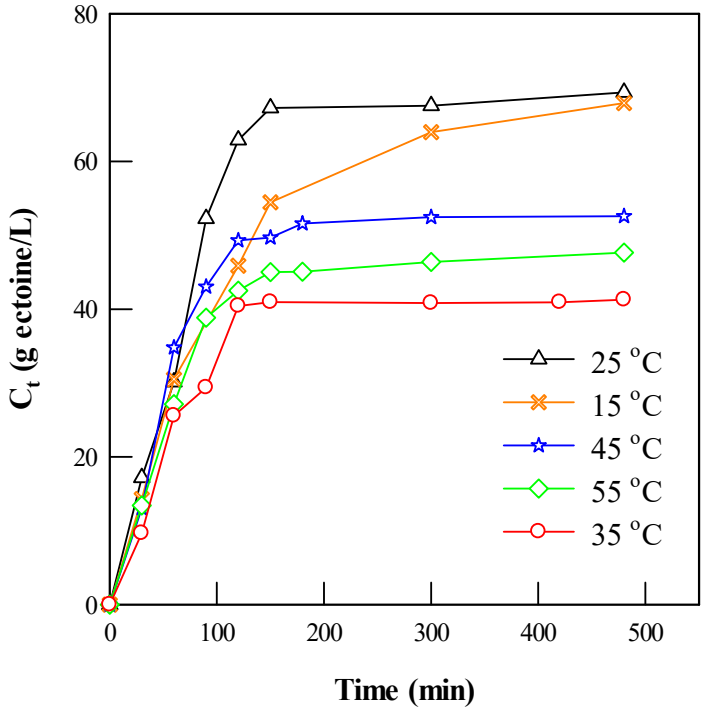


**Figure 11.** Effect of time on ectoine desorption from Dowex® HCR-S with different temperatures (saturated resin/NaOH solution = 0.1 g/mL, NaOH concentration: 0.5 mol/L).

4.3.4. Desorption Kinetics of Ectoine from the Ion-Exchange Resin

Mathematical modeling of experimental data from the batch reactor was undertaken to construct a robust and trustworthy mathematical model that could predict the kinetics of desorption in a fixed-bed column [36]. Table 7 shows the desorption results using the external diffusion model (EDM); the simulated parameters were not reliable based on the unstable $R^2$. Except for the data under 35 °C, the EDM rate constant, $k_d$, had an average value of 1.13 $min^{-1}$, and the ectoine desorption was more favorable under lower temperatures. More desorption kinetic models are required for the investigation of ectoine desorption in order to find the rate-limiting step.

**Table 7.** Parameters of the external solid diffusion model calculated at different temperatures.

| Temp.(°C) | $k_d$ ($min^{-1}$) | $R^2$ |
|---|---|---|
| 15 | 0.31 | 0.92 |
| 25 | 1.08 | 0.82 |
| 35 | 4.90 | 0.64 |
| 45 | 1.64 | 0.91 |
| 55 | 1.48 | 0.98 |

4.3.5. Mechanism of Ectoine Desorption from Ion-Exchange Resin

Desorption using the ion-exchange method can be classified into two types: pH desorption and salt desorption. Desorption of amino acid depending on pH value is built on the use of the isoelectric point of its nature. When the pH value is over the pI of ectoine, the anionic form is exhibited. In contrast, the cationic form is shown when the pH is below its pI. As for salt desorption, by using the exchange priority depending on their affinity towards ion-exchanging sites, salt ions with a stronger affinity compete with targeting analytes, and thus, analytes can be exchanged out. The effect of pH (Section 4.1.1) and NaOH concentration (Section 4.1.2) on ectoine desorption shows that the desorption strengthened with the increase of the $OH^-$ concentration. Moreover, ectoine desorption

relies on the mechanism of pH desorption, with 90% desorption. NaOH solution can promote a strong ectoine removal, resulting in favorable desorption.

Figure 12 shows that the desorption efficiency when using NaCl (54.5%) was not as high as when using NaOH (78.1%) at 35 °C. The desorption of ectoine showed a higher rate in the first 120 min when using NaCl, based on the mechanism of salt desorption, and a higher equilibrium desorption was obtained by using NaOH, which relies on both pH and salt desorption. Therefore, NaOH promotes stronger desorption of ectoine than NaCl since there are two mechanisms that support using NaOH as a desorption agent.

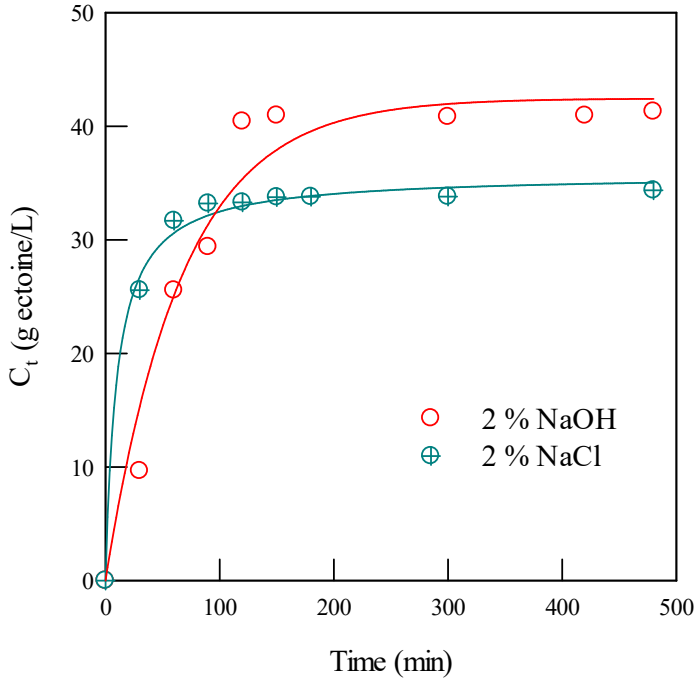


**Figure 12.** Comparison of NaOH and NaCl in ectoine desorption (temperature: 35 °C).

According to the results of the isotherm analysis, the adsorption of ectoine using Dowex strong-acid cation-exchange resin achieved the best fit to the Sips model, implying that the sorption process is built on both ion exchange and physisorption. Ectoine desorption from the saturated resin using NaOH as a desorbed agent was assumed to have three steps, based on the sorption phenomena and desorption results: concentration-dependent desorption, salt desorption, and pH desorption (Figure 13). The desorption of ectoine under pH values ranging from 2 to 6 was an average of 7.63%, as shown in Table 5. Physisorption resulted in concentration-dependent desorption of ectoine. Secondly, an NaCl solution was applied to the ectoine desorption, represented by salt desorption, obtaining 54.5% desorption under neutral conditions. Finally, using NaOH solution as a pH desorption strategy, the best ectoine desorption reached (89.7%). Van der Waals desorption (concentration desorption) was weaker than electrostatic desorption (salt and pH desorption), and this supports the sorption theory that physisorption is more accessible than ion exchange. Therefore, ectoine desorption using NaOH solution included ion exchange mechanisms as the significant driving force to repel ectoine from the ion-exchanger phase (pH and salt desorption) and concentration-dependent desorption.

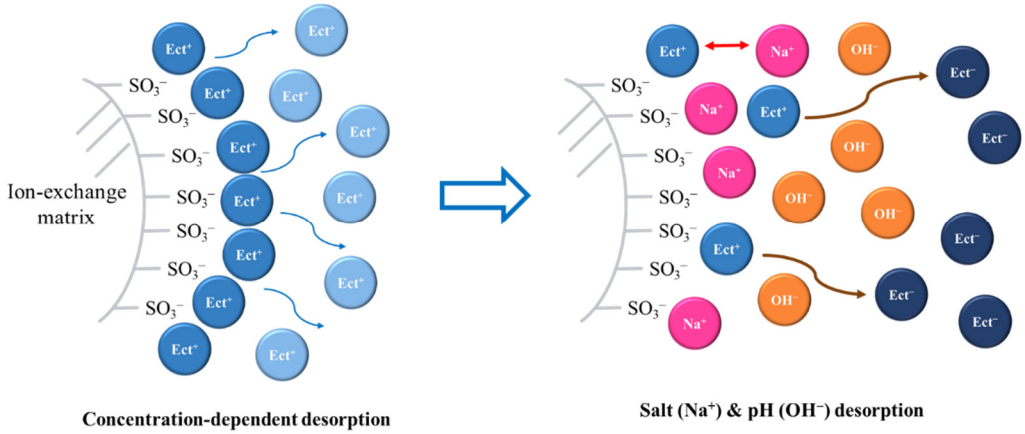


**Figure 13.** Mechanism of ectoine desorption using Dowex® HCR-S. **: adsorbed ectoine ion, **: free ectoine ion, **: sodium ion, **: hydroxide ion**

## 5. Conclusions

In this research, adsorption, saturation, and desorption were utilized to capture ectoine using ion-exchange resin in a batch system in order to investigate ectoine's adsorption/desorption behavior. Regression of isotherms and kinetic models were carried out to elucidate the adsorption behavior and optimum operating conditions. The analysis results showed that the adsorption of ectoine using Dowex® HCR-S resin fits best when using the Sips isotherm. Thus, the ectoine adsorption mechanism is ion exchange, based on electrostatic force (monolayer), and physisorption based on van der Waal's force (multilayer). Moreover, the effect of temperature indicates that the adsorption of ectoine can be divided into two outcomes: group I (25 °C~45 °C) was exothermic, and group II (45 °C~65 °C) was endothermic. In group I, ectoine adsorption is more favorable at lower temperatures, establishing physisorption. In group II, adsorption uptake is enhanced at higher temperatures, supporting ion exchange via the Coulomb force. For the kinetic study, the results indicate that pseudo-second-order models could explain the ectoine adsorption reaction using Dowex® HCR-S resin, and the activation energy was 36.5 kJ $mol^{-1}$. The intraparticle diffusion model can explain the kinetic mechanism for the multilinear plot and the resin structure (gel-type). The values of ΔG, ΔH, and ΔS were also calculated. The negative values of ΔG at the experimental temperatures indicate that the adsorption was spontaneous, and the negative values of ΔH and ΔS show that the adsorption was exothermic. The randomness decreased during adsorption for group I but increased for group II.

The saturation of ectoine on Dowex® HCR-S resin was independent of both temperature and resin dosage. On average, the saturation capacity was 0.58 g/g, with 93.6% adsorption using 125 g/L of initial ectoine concentration. Desorption of ectoine reached 89.7% of desorption with 0.51 g under an NaOH concentration of 0.5 mol/L and at 15 °C. Comparing the desorbed agent with both NaOH and NaCl, more ectoine ions were desorbed using NaOH, which confirmed that both pH and salt desorption are the mechanisms of ectoine desorption. The thermodynamic and kinetic parameters obtained from this study can be used for adsorption/desorption of the fix-bed column, designed for larger-scale production. The optimal condition of separating the ectoine from the fermentation broth in a fix-bed column can reduce the separation cost of ectoine.

**Author Contributions:** Conceptualization, Y.-C.W., Y.-H.W. and H.-S.W.; methodology, Y.-C.W.; formal analysis, Y.-C.W.; investigation, Y.-C.W.; writing—original draft preparation, Y.C.W.; writing—review and editing, H.-S.W.; supervision, H.-S.W. All authors have read and agreed to the published version of the manuscript.

**Funding:** We thank the Ministry of Science and Technology of Taiwan for financially supporting this study under grant number MOST 104-2632-E-155 -001, 105-2632-E-155 -001, 106-2632-E-155 -001.

**Institutional Review Board Statement:** Not applicable.

**Informed Consent Statement:** Not applicable.

**Conflicts of Interest:** The authors declare no conflict of interest.

## References


1. Becker, J.; Wittmann, C. Microbial production of extremolytes—High-value active ingredients for nutrition, health care, and well-being. *Curr. Opin. Biotechnol.* **2020**, *65*, 118–128, doi:10.1016/j.copbio.2020.02.010.
2. Chen, R.; Zhu, L.; Lv, L.; Yao, S.; Li, B.; Qian, J. Optimization of the extraction and purification of the compatible solute ectoine from Halomonas elongate in the laboratory experiment of a commercial production project. *World J. Microbiol. Biotechnol.* **2017**, *33*, 116, doi:10.1007/s11274-017-2281-y.
3. Kunte, H.J.; Lentzen, G.; Galinski, E.A. Industrial Production of the Cell Protectant Ectoine: Protection Mechanisms, Processes, and Products. *Curr. Biotechnol.* **2014**, *3*, 10–25.
4. Pastor, J.M.; Salvador, M.; Argandoña, M.; Bernal, V.; Reina-Bueno, M.; Csonka, L.N.; Iborra, J.L.; Vargas, C.; Nieto, J.J.; Cánovas, M. Ectoines in cell stress protection: Uses and biotechnological production. *Biotechnol. Adv.* **2010**, *28*, 782–801, https://doi.org/10.1016/j.biotechadv.2010.06.005.
5. Behazin, R.; Ebrahimi, A. The physicochemical properties and tyrosinase inhibitory activity of ectoine and its analogues: A theoretical study. *Comput. Theor. Chem.* **2018**, *1130*, 6–14, https://doi.org/10.1016/j.comptc.2018.03.003.
6. Zhao, Q.; Li, S.; Lv, P.; Sun, S.; Ma, C.; Xu, P.; Su, H.; Yang, C. High ectoine production by an engineered Halomonas hydrothermalis Y2 in a reduced salinity medium. *Microb. Cell Factories* **2019**, *18*, 184, https://doi.org/10.1186/s12934-019-1230-x.
7. Chen, W.-C.; Hsu, C.-C.; Lan, J.C.-W.; Chang, Y.-K.; Wang, L.-F.; Wei, Y.-H. Production and characterization of ectoine using a moderately halophilic strain Halomonas salina BCRC17875. *J. Biosci. Bioeng.* **2018**, *125*, 578–584, doi:10.1016/j.jbiosc.2017.12.011.
8. Chen, W.-C.; Yuan, F.-W.; Wang, L.-F.; Chien, C.-C.; Wei, Y.-H. Ectoine production with indigenous Marinococcus sp. MAR2 isolated from the marine environment. *Prep. Biochem. Biotechnol.* **2020**, *50*, 74–81, doi:10.1080/10826068.2019.1663534.
9. Chen, J.; Liu, P.; Chu, X.; Chen, J.; Zhang, H.; Rowley, D.C.; Wang, H. Metabolic pathway construction and optimization of Escherichia coli for high-level ectoine production. *Curr. Microbiol.* **2020**, 77, 1412–1418, https://doi.org/10.1007/s00284-020-01888-6.
10. Sauer, T.; Galinski, E.A. Bacterial milking: A novel bioprocess for production of compatible solutes. *Biotechnol. Bioeng.* **1998**, *57*, 306–313, https://doi.org/10.1002/(SICI)1097-0290(19980205)57:3<306::AID-BIT7>3.0.CO;2-L.
11. Gießelmann, G.; Dietrich, D.; Jungmann, L.; Kohlstedt, M.; Jeon, E.J.; Yim, S.S.; Sommer, F.; Zimmer, D.; Mühlhaus, T.; Schroda, M. Metabolic engineering of Corynebacterium glutamicum for high-level ectoine production: Design, combinatorial assembly, and implementation of a transcriptionally balanced heterologous ectoine pathway. *Biotechnol. J.* **2019**, *14*, 1800417, https://doi.org/10.1002/biot.201800417.
12. Lang, Y.-j.; Bai, L.; Ren, Y.-n.; Zhang, L.-h.; Nagata, S. Production of ectoine through a combined process that uses both growing and resting cells of Halomonas salina DSM 5928 T. *Extremophiles* **2011**, *15*, 303–310.
13. Fülberth, K.; Müssig, H.; Wesp, B. Method for the chromatographic isolation of ectoine, European Patent EP1461322A1. 2004.
14. LeVan, M.D.; Carta, G.; Yon, C.M. Adsorption and ion exchange. *Energy* **1997**, *16*, 17.
15. Lagergren, S. Zur theorie der sogenannten adsorption geloster stoffe. *K. Sven. Vetenskapsakademiens. Handl.* **1898**, *24*, 1–39.
16. Vadivelan, V.; Kumar, K.V. Equilibrium, kinetics, mechanism, and process design for the sorption of methylene blue onto rice husk. *J. Colloid Interface Sci.* **2005**, *286*, 90–100, https://doi.org/10.1016/j.jcis.2005.01.007.
17. Ho, Y.S. Removal of copper ions from aqueous solution by tree fern. *Water Res.* **2003**, *37*, 2323–2330, https://doi.org/10.1016/S0043-1354(03)00002-2.
18. Weber, W.J.; Morris, J.C. Kinetics of adsorption on carbon from solution. *J. Sanit. Eng. Div.* **1963**, *89*, 31–60.
19. Wu, F.C.; Tseng, R.L.; Juang, R.S. Initial behavior of intraparticle diffusion model used in the description of adsorption kinetics. *Chem. Eng. J.* **2009**, *153*, 1–8, https://doi.org/10.1016/j.cej.2009.04.042.
20. McKay, G.; Otterburn, M.; Sweeney, A. The removal of colour from effluent using various adsorbents—III. Silica: Rate processes. *Water Res.* **1980**, *14*, 15–20, https://doi.org/10.1016/0043-1354(80)90037-8.
21. Aharoni, C.; Tompkins, F. Kinetics of adsorption and desorption and the Elovich equation. In *Advances in Catalysis*; Elsevier: Amsterdam, The Netherlands, 1970; Volume 21, pp. 1–49.
22. Wu, F.C.; Tseng, R.L.; Juang, R.S. Characteristics of Elovich equation used for the analysis of adsorption kinetics in dye-chitosan systems. *Chem. Eng. J.* **2009**, *150*, 366–373, https://doi.org/10.1016/j.cej.2009.01.014.
23. Dada, A.; Olalekan, A.; Olatunya, A.; Dada, O. Langmuir, Freundlich, Temkin and Dubinin–Radushkevich isotherms studies of equilibrium sorption of Zn2+ unto phosphoric acid modified rice husk. *IOSR J. Appl. Chem.* **2012**, *3*, 38–45, http://doi.org/10.9790/5736-0313845.
24. Weber, T.W.; Chakravorti, R.K. Pore and solid diffusion models for fixed-bed adsorbers. *AIChE J.* **1974**, *20*, 228–238, https://doi.org/10.1002/aic.690200204.
25. Prasad, R.K.; Srivastava, S. Sorption of distillery spent wash onto fly ash: Kinetics and mass transfer studies. *Chem. Eng. J.* **2009**, *146*, 90–97, https://doi.org/10.1016/j.cej.2008.05.021.

26. Osmari, T.A.; Gallon, R.; Schwaab, M.; Barbosa-Coutinho, E.; Severo Jr, J.B.; Pinto, J.C. Statistical analysis of linear and non-linear regression for the estimation of adsorption isotherm parameters. *Adsorpt. Sci. Technol.* **2013**, *31*, 433–458, https://doi.org/10.1260/0263-6174.31.5.433.
27. Al-Ghouti, M.A.; Da'ana, D.A. Guidelines for the use and interpretation of adsorption isotherm models: A review. *J. Hazard. Mater.* **2020**, 122383, https://doi.org/10.1016/j.jhazmat.2020.122383.
28. Freundlich, H.M.F. Over the adsorption in solution. *J. Phys. Chem* **1906**, *57*, 385.
29. Ho, Y.S. *Absorption of Heavy Metals from Waste Streams by Peat*; University of Birmingham: Birmingham, UK, 1995.
30. Dubinin, M. The potential theory of adsorption of gases and vapors for adsorbents with energetically nonuniform surfaces. *Chem. Rev.* **1960**, *60*, 235–241, https://doi.org/10.1021/cr60204a006.
31. Langmuir, I. The constitution and fundamental properties of solids and liquids. Part I. Solids. *J. Am. Chem. Soc.* **1916**, *38*, 2221–2295, https://doi.org/10.1021/ja02268a002.
32. Redlich, O.; Peterson, D.L. A useful adsorption isotherm. *J. Phys. Chem.* **1959**, *63*, 1024–1024, http://doi.org/10.1021/j150576a611.
33. Sips, R. On the Structure of a Catalyst Surface. *J. Chem. Phys.* **1948**, *16*, 490–495, http://doi.org/10.1063/1.1746922.
34. Temkin, M.I. Kinetics of ammonia synthesis on promoted iron catalysts. *Acta Physiochim. URSS* **1940**, *12*, 327–356.
35. Inglezakis, V.J.; Zorpas, A.A. Heat of adsorption, adsorption energy and activation energy in adsorption and ion exchange systems. *Desalination Water Treat.* **2012**, *39*, 149–157, https://doi.org/10.1080/19443994.2012.669169.
36. Staudt, J.; Scheufele, F.B.; Ribeiro, C.; Sato, T.Y.; Canevesi, R.; Borba, C.E. Ciprofloxacin desorption from gel type ion exchange resin: Desorption modeling in batch system and fixed bed column. *Sep. Purif. Technol.* **2020**, *230*, 115857, https://doi.org/10.1016/j.seppur.2019.115857.
37. Ismail, M.; Hanafiah, K.M. Kinetic, isotherm, and possible mechanism of Pb (II) ion adsorption onto xanthated neem (Azadirachta indica) leaf powder. *Sains Malays.* **2020**, *49*, 1585–1596, http://dx.doi.org/10.17576/jsm-2020-4907-11.
38. Nagy, B.; Mânzatu, C.; Măicăneanu, A.; Indolean, C.; Barbu-Tudoran, L.; Majdik, C. Linear and nonlinear regression analysis for heavy metals removal using Agaricus bisporus macrofungus. *Arab. J. Chem.* **2017**, *10*, S3569–S3579, https://doi.org/10.1016/j.arabjc.2014.03.004.
39. Bulut, Y.; Aydın, H. A kinetics and thermodynamics study of methylene blue adsorption on wheat shells. *Desalination* **2006**, *194*, 259–267, https://doi.org/10.1016/j.desal.2005.10.032.
40. Aksu, Z.; Kutsal, T. A bioseparation process for removing lead (II) ions from waste water by using C. vulgaris. *J. Chem. Technol. Biotechnol.* **1991**, *52*, 109–118, https://doi.org/10.1002/jctb.280520108.
41. Kajjumba, G.W.; Emik, S.; Öngen, A.; Özcan, H.K.; Aydın, S. Modelling of adsorption kinetic processes—errors, theory and application. In *Advanced Sorption Process Applications*; IntechOpen: London, UK, 2018.